https://doi.org/10.1139/cgj-2017-0343

Modelling effects of recent suction history on small-strain stiffness of unsaturated soil

Authors: R. Kaewsong, C. Zhou* and C. W. W. Ng

*Corresponding author

Information of the authors

First author: Ms R. Kaewsong

Research student, Department of Civil and Environmental Engineering, the Hong Kong University of Science and Technology, Clear Water Bay, Kowloon, Hong Kong

E-mail: rkaewsong@connect.ust.hk

Co-author: Dr C. Zhou

Research assistant professor, Department of Civil and Environmental Engineering, the Hong Kong University of Science and Technology, Clear Water Bay, Kowloon, Hong Kong

E-mail: czhou@connect.ust.hk

Co-author: Dr C. W. W. Ng

Chair professor, Department of Civil and Environmental Engineering, the Hong Kong University of Science and Technology, Clear Water Bay, Kowloon, Hong Kong

E-mail: cecwwng@ust.hk

Abstract

Recent suction history is found affecting shear modulus of unsaturated soil at small strains (i.e. from 0.001 to 1%). In this study, a bubble model for unsaturated soil is developed within the framework of kinematic hardening and bounding surface plasticity. An elliptical elastic bubble is defined inside a modified Cam-clay bounding surface. Being a key feature of the proposed model, size of the elastic bubble is modelled as a function of suction, degree of saturation and plastic volumetric strain. Translation of the elastic bubble is governed by suction, degree of saturation and stress increments. Moreover, hardening modulus depends on not only stress and void ratio but also suction, degree of saturation and relative position of the elastic bubble and the bounding surface. The proposed model is evaluated using suction-controlled constant-*p* shear tests on completely decomposed tuff (silt). It is evident that the new model is capable of well capturing effects of recent suction history on non-linear stress-strain relation and shear modulus degradation at small strains.

Keywords

Unsaturated soil; constitutive model; small-strain modulus

Introduction

To describe the behaviour of unsaturated soil, many elastoplastic models have been proposed in the past three decades (e.g. Alonso et al., 1990; Wheeler et al., 2003; Alonso et al., 2013; Zhou & Sheng, 2015; Lloret-Cabot et al., 2017). Some important aspects, such as wetting-induced collapse, increases in yield stress and shear strength with increasing suction, are well captured. Recently, effects of recent suction history are found significantly affecting small-strain stiffness of unsaturated soil (Ng & Xu, 2012).

To simulate small-strain behaviour of unsaturated soil, Wong & Masin (2014) developed a new constitutive model using the hypoplasticity framework. The intergranular strain concept (Niemunis and Herle, 1997) was extended to model elastic threshold strain at unsaturated condition. On the other hand, Zhou et al. (2015a) proposed a bounding surface plasticity model to simulate small-strain stiffness of unsaturated soil. Two different plastic mechanisms, including constant-p shearing and constant stress ratio compression, were incorporated. Only the first plastic mechanism considers the influence of recent history of stress ratio.

In this study, a constitutive model for unsaturated soil is newly developed to simulate the effects of recent suction history on small-strain behaviour. A key feature of the new model is the dependency of the kinematic-hardening elastic bubble and hardening modulus on current suction, degree of saturation, stress state as well as yield stress. The capability of the proposed model is verified with experimental results of completely decompose tuff (CDT) (Ng & Xu, 2012).

Mathematical formulations

Constitutive variables

The proposed model is formulated in the triaxial space in terms of average skeleton stress (p^*), bonding variable (ξ) and deviatoric stress (q). The average skeleton stress is equivalent to mean Bishop's effective stress, accounting for the average stress acting on soil skeleton through mean net stress and average pore fluid pressure. As proposed by Gallipoli et al. (2003), the bonding variable is used in describing stabilizing effects of meniscus water on soil skeleton. Detailed definitions of these variables are summarized in the Appendix.

Bounding surface (BS)

The elastoplastic behaviour of soil is modelled using the bounding surface plasticity framework (Dafalias, 1986). Within this framework, a "bubble model" for saturated soil proposed by Al-Tabbaa & Wood (1989) is extended to simulate small-strain behaviour of unsaturated soil. Figure 1 shows a schematic diagram of the bounding surface in the $p^* - q - \xi$ space. At a given ξ, the BS is equivalent to yield surface as used in the modified Cam-clay model.

$$F_{BS} = \left(p^* - \frac{p^*_{0,\xi}}{2}\right)^2 + \frac{q^2}{M^2} - \frac{{p^*_{0,\xi}}^2}{4} \quad (1)$$

where M is the critical state stress ratio. $p^*_{0,\xi}$ is the yield stress at a given ξ, accounting for a change in yield stress with suction and degree of saturation. It can be calculated from the yield stress at saturated state and normal compression lines (NCLs) at various ξ (see equations (17)-(19) in the Appendix).

Elastic bubble (EB)

The EB, which bounds the purely elastic region (i.e. equations (20)-(22)), is assumed to have the same shape as the BS:

$$F_{EB} = (p^* - p^*_\alpha)^2 + \frac{(q - q_\alpha)^2}{M^2} - \frac{R^2 {p^*_{0,\xi}}^2}{4} \quad (2)$$

where (p_α^* , q_α) is the centre of the EB; R is the ratio between the size of the EB to that of the BS.

As a key feature of the current model, kinematic hardening law is adopted for the EB to record the recent loading history of soil. It should be noted the proposed model uses a single kinematic yield surface to consider effects of suction and stress on small strain behaviour. The predictions are thus considered as an approximation. To better capture the influence of recent suction and stress history, an additional kinematic history surface (Stallebrass and Taylor, 1997) should be adopted in future. Given a basic constraint that the EB and the BS must not intersect, the EB must translate along the vector D connecting the "actual" stress (p^*, q) on the EB and the "image" stress (p_i^*, q_i) on the BS (i.e. equations (23)-(24)). In addition, these two stress state points have the same normal vector. The mapping rule of the EB is expressed as

$$\begin{bmatrix} dp_\alpha^* \\ dq_\alpha \end{bmatrix} = dp_{0,\xi}^* \begin{bmatrix} \frac{p_\alpha^*}{p_{0,\xi}^*} \\ \frac{q_\alpha}{p_{0,\xi}^*} \end{bmatrix} + S \begin{bmatrix} p_i^* - p^* \\ q_i - q \end{bmatrix} \tag{3}$$

where S is the translation distance along the vector D. From the mapping rule and consistency condition of the EB, S is described by

$$S = \frac{1}{-\frac{\partial F_{EB}}{\partial p_\alpha^*}(p_i^* - p^*) - \frac{\partial F_{EB}}{\partial q_\alpha}(q_i - q)} \left(\frac{\partial F_{EB}}{\partial p^*} dp^* + \left(\frac{\partial F_{EB}}{\partial p_\alpha^*} \frac{p_\alpha^*}{p_{0,\xi}^*} + \frac{\partial F_{EB}}{\partial q_\alpha} \frac{q_\alpha}{p_{0,\xi}^*} + \frac{\partial F_{EB}}{\partial p_{0,\xi}^*} \right) dp_{0,\xi}^* + \frac{\partial F_{EB}}{\partial q} dq \right) \tag{4}$$

Hardening modulus

The hardening modulus is formulated in two scenarios. In the first scenario, the EB and the BS are in contact. Plastic strain increments (i.e. $d\varepsilon_v^p$ and $d\varepsilon_q^p$) are determined from flow rule

(assumed to be associated in the current study, see equation (25)), hardening laws and consistency condition of the EB and the BS as follows:

$$\begin{bmatrix} d\varepsilon_v^p \\ d\varepsilon_q^p \end{bmatrix} = \frac{1}{h}\begin{bmatrix} \frac{\partial F_{EB}}{\partial p^*} \\ \frac{\partial F_{EB}}{\partial q} \end{bmatrix}\begin{bmatrix} \frac{\partial F_{EB}}{\partial p^*} & \frac{\partial F_{EB}}{\partial q} & \left(\frac{\partial F_{EB}}{\partial p_\alpha^*}\frac{p_\alpha^*}{p_{0,\xi}^*} + \frac{\partial F_{EB}}{\partial q_\alpha}\frac{q_\alpha}{p_{0,\xi}^*} + \frac{\partial F_{EB}}{\partial p_{0,\xi}^*}\right)\frac{\partial p_{0,\xi}^*}{\partial \frac{e}{e_s}}\frac{d\frac{e}{e_s}}{d\xi} \end{bmatrix}\begin{bmatrix} dp^* \\ dq \\ d\xi \end{bmatrix} \tag{5}$$

where h is the scalar plastic modulus and is expressed as

$$h = h_0 = \left(\frac{\partial F_{EB}}{\partial p_\alpha^*}\frac{p_\alpha^*}{p_{0,\xi}^*} + \frac{\partial F_{EB}}{\partial q_\alpha}\frac{q_\alpha}{p_{0,\xi}^*} + \frac{\partial F_{EB}}{\partial p_{0,\xi}^*}\right)\frac{\partial p_{0,\xi}^*}{\partial p_0^*}\left(\frac{\partial p_0^*}{\partial \varepsilon_v^p}\frac{\partial F_{EB}}{\partial p^*} + \frac{\partial p_0^*}{\partial \varepsilon_q^p}\frac{\partial F_{EB}}{\partial q}\right) \tag{6}$$

where h_0 is the scalar plastic modulus at the condition where the BS and the EB are in contact.

In the second scenario, where the EB moves within the BS, plastic modulus h is modified to account for the distance between EB and BS.

$$h = h_0 + H \tag{7}$$

where H is the additional modulus quantity. In the present model, the formulation for H is modified from Al-Tabbaa & Wood (1989) to consider the influence of soil suction and degree of saturation.

$$H = \delta\frac{(1+e_0)}{(\lambda_\xi - \kappa)}\left(\frac{d_1}{2d_{1,max} - d_1}\right)^\phi \left(p_{0,\xi}^*(1+\xi)^\alpha\right)^3 \tag{8}$$

where ϕ, α and δ are soil parameters relating to the rate of modulus degradation; d_1 is the product of the vector D and the normal vector on the EB at the current stress state. The variable d_1 can be determined by

$$d_1 = \frac{2}{Rp^*_{0,\xi}}\left[(p^* - p^*_\alpha)(p^*_i - p^*) + \frac{(q - q_\alpha)}{M^2}(q_i - q)\right] \quad (9)$$

where $d_{1,max}$ is the maximum value of d_1 determined the stress state at which plastic straining first occurred since the last loading reversal.

Water retention behaviour

Water retention behaviour of unsaturated soil is modelled within the framework of bounding surface plasticity. As shown in Figure 2, the main drying and wetting curves serve as bounding surfaces in the $s - S_r$ plane. These BS surfaces describe S_r as a function of suction and void ratio (i.e. equation (26)) (Gallipoli, 2012). Following Zhou et al. (2012), a change in the S_r inside the main surfaces is a function of the slope of the BS surfaces $\left(\frac{dS_r}{ds}\right)_{s=s_d}$ and $\left(\frac{dS_r}{ds}\right)_{s=s_w}$ at the "image" suction s_d and s_w. For drying scanning,

$$\frac{dS_r}{ds} = \left(\frac{dS_r}{ds}\right)_{s=s_d}\left(\frac{s - s_r}{s_d - s_r}\right)^\beta \quad (10)$$

Similarly, the wetting scanning curve is governed by

$$\frac{dS_r}{ds} = \left(\frac{dS_r}{ds}\right)_{s=s_w}\left(\frac{s_r - s}{s_r - s_w}\right)^\beta \quad (11)$$

where s_r is the suction at which last hydro-loading reversal occurs, accounting for the effects of recent suction history on water retention behaviour.

Experimental program and model calibration

The new model is used to simulate three series of suction-controlled constant-p shear tests on CDT, as reported by Ng and Xu (2012) and Zhou et al. (2015b). Figure 3(a) shows stress paths of the first series of tests for investigating effect of suction magnitude on small-strain behaviour. In this series, three specimens (S1, S150 and S300) were compressed to mean net

stress of 100 kPa. Subsequently, a predefined suction of 1, 150 or 300 kPa was applied from the initial suction of 95 kPa. Finally, the specimen was sheared at constant mean net stress and suction. Effect of suction history on stiffness degradation was investigated through comparing between the tests S150C2 and S150 in the second series (Fig. 3(b)). After isotropic compression to 100 kPa, specimen S150 was dried to 150 kPa and then sheared at constant suction and mean net stress. On the contrary, the specimen S150C2 was dried to a suction of 300 kPa, wetted to 150 kPa and then sheared. Effect of recent suction history was investigated through the third series of tests, as summarized in Fig. 3(c). After isotropic compression to 100 kPa, the two specimens (S150C2D30 and S150C2D60) were dried to a suction of 300 kPa and wetted to 150 kPa. Then, the specimens S150C2D30 and S150C2D60 were subjected to additional suction decrements of 30 and 60 kPa, respectively. Finally, each specimen was dried back to 150 kPa and sheared at constant mean net stress and suction. Basic properties of CDT are shown in Table. 1.

The value of model parameters for CDT is shown in Table 2. The parameters λ, N, a and b are determined from the NCL at different suctions reported in Ng & Yung (2008). The critical state stress ratio M is as reported in Zhou et al. (2015). The parameters m, n, ω_d, ω_w and β are obtained by fitting the water retention curves reported in Ng et al. (2012). The values of parameters C_0 and n_s, which describe effects of structure and ξ on G_0 respectively, are calibrated through measured G_0 along suction-controlled compression. The parameters R, δ, ϕ and α are obtained by fitting the stress-strain relations and shear modulus degradation reported in Ng & Xu (2012).

Comparisons between measured and computed results

Figure 4(a) compares measured and computed stress-strain relations of unsaturated CDT at suctions of 1, 150 and 300 kPa. Nonlinearity of the stress-strain curves at strains ranging

between 0.001 and 1% is well captured, mainly because plastic strain is allowed inside the BS. At a given deviatoric strain, the model well predicts a stiffer response at a higher suction. According to equations (12) and (13), average skeleton stress and bonding variable are larger at a higher suction. Hence, initial shear stiffness and hardening modulus increase with an increasing suction (i.e. equation (8), (17) and (22)).

Figure 4(b) shows the small-strain shear moduli at suctions of 1, 150 and 300 kPa. When deviatoric strain increases from 0.001% to 0.003%, soil stiffness maintains almost constant at suction of 300 kPa but decreases by about 25% at suction of 150 kPa. The influence of suction on stiffness degradation within this strain range is reasonably well captured by the proposed model. The new model overestimates the elastic-threshold strain at suction of 1 kPa, due to an overestimation of the size of the EB at low suction range. The prediction error could be minimized by modelling the size ratio (R) between the EB and the BS as a function of ξ. It should be pointed out that, however, consideration of R as a function of ξ may induce difficulties in finding seasonable parameters to capture soil behaviour at both saturated and unsaturated conditions. Any future work on this issue should ensure unified modelling of saturated and unsaturated soil behaviour. In the current note, no further modification is introduced to further improve the predictions at suction of 1 kPa. Further modifications are needed in future to improve the model.

Figure 5 shows the measured and computed effects of suction history. The model well predicts the stiffer response in the specimen experienced a higher suction history. This is because a cycle of drying-wetting lead to an irreversible increase in ξ, resulting in a larger EB and BS (i.e. equations (17) and (19)). Moreover, the specimen with a higher suction history becomes overconsolidated due to the accumulation of plastic contraction. Consequently, its stress state is inside the EB before shearing. It should be noted that the model predictions and experimental results of compacted CDT are slightly different. The model prediction could be

155 further improved by incorporating anisotropy (e.g., Stropeit et al. 2008; D'Onza et al. 2011;
156 Al-Sharrad & Gallipoli 2014; Li et al., 2017) and non-associated flow rule (Lai et al., 2016).

157 Figure 6 shows the effects of recent suction history. The model correctly predicts that
158 the specimen with a smaller additional suction decrement (S150C2D30) exhibits stiffer
159 response than that with a larger decrement (S150C2D60). According to the model prediction,
160 these additional suction decrements lead to a relocation of the EB (see equations (3)-(4)). The
161 EB of specimen S150C2D60 translated more than specimen S150C2D30. Before shearing,
162 stress state of specimen S150C2D60 is closer to the boundary of the EB. This illustrates that
163 kinematic hardening yield surface and its dependency on suction, degree of saturation, stress
164 state and plastic volumetric strain are essential for properly modelling the effects of recent
165 suction history. In addition, a recent suction history may not be accurately predicted if there
166 is no elastic range for compression (Zhou et al., 2015a). Even though effects of recent suction
167 history is fairly captured by the new model, there are discrepancy between measured and
168 predicted elastic-threshold strain of specimen S150C2D60. This problem is likely because the
169 influence of ξ on the size of the EB is not incorporated. As discussed earlier, the prediction
170 could be improved by modelling the size ratio (R) between EB and BS as a function of ξ.

171 Figure 7 shows effects of recent drying and wetting history on small strain stiffness.
172 The specimens with additional drying and wetting history (S150C2I30 and S150C2I100)
173 exhibit very similar responses to that without additional drying and wetting history (S150C2).
174 The difference induced by additional drying and wetting history is less than 10%. This is
175 different from the results of tests S150C2D30 and S150C2D60, in which additional wetting
176 and drying history shows significant influence on small strain stiffness (see Figure 6). The
177 observed differences in Figures 6 and 7 can be well explained using the new model. In tests
178 S150C2I30 and S150C2I100, soil state moves along the scanning curves during the
179 additional drying and wetting process. Relocation of the EB is negligible because stress paths

180 are within the EB. In tests S150C2D30 and S150C2D60, soil state moves along the main
181 wetting curve and scanning drying curve during the additional wetting and drying process.
182 Recent suction changes lead to translation of the EB (i.e., kinematic hardening) and thus
183 greatly affect the stiffness degradation curve.

184 It has to be noted that significant features of soil deformation include not only
185 stiffness but also dilatancy, which mainly depend on elastic and plastic deformations,
186 respectively. The current note focuses on soil behaviour at small strains (less than 1%).
187 Within this strain range, plastic modulus is relatively high (see equations (6) to (8)) and hence
188 plastic deformation would be minimal. A simple flow rule, which considers dilatancy as a
189 function of stress ratio only, is therefore used for simplicity. It should be worthwhile to apply
190 state-dependent dilatancy (Chiu and Ng, 2003) to extend the new model for large strains in
191 the future.

192 ## Summary and conclusions

193 A kinematic hardening bubble model is proposed to simulate effects of recent suction history
194 on small-strain stiffness of unsaturated soil. Some new formulations are proposed for the
195 hardening laws of the elastic bubble and the hardening modulus, which are both related to
196 suction, degree of saturation, stress state and plastic volumetric strain.

197 The proposed model is verified using three series of suction-controlled constant-p
198 shear tests on unsaturated compacted completely decomposed tuff (silt). Computed stress-
199 strain relation and shear modulus degradation curve are fairly consistent with experimental
200 results. Effects of suction magnitudes, suction histories and recent suction histories on
201 unsaturated soil behaviour at small strains are captured.

202 ## Acknowledgements

The authors would like to acknowledge the financial support provided by the Research Grants Council of the Hong Kong Special Administrative Region (HKSAR) through the research grants 16216116, 616812 and T22-603/15N. In addition, the research grant 51509041 provided by the National Science Foundation of China is also gratefully acknowledged.

Appendix: Summary of model formulations not specified in the main text

(a) Constitutive variables

$$p^* = (p - u_a) + S_r \cdot s \tag{12}$$

$$\xi = f(s)(1 - S_r) \tag{13}$$

where

$$s = u_a - u_w \tag{14}$$

$$S_r = \frac{wG_s}{e} \tag{15}$$

$$f(s) = \frac{3T_s}{rs}\frac{\left(\sqrt{9 + 8rs/T_s} - 3\right)\left(\sqrt{9 + 8rs/T_s} + 1\right)}{4} \tag{16}$$

(b) Yield stress at a given ξ

$$p^*_{0,\xi} = 100exp\left(\frac{N_\xi - N + (\lambda - \kappa)\ln(p^*_0/100)}{\lambda_\xi - \kappa}\right) \tag{17}$$

where

$$\frac{N_\xi}{N} = \frac{\lambda_\xi}{\lambda} = \frac{e}{e_s} \tag{18}$$

$$\frac{e}{e_s} = 1 - a \cdot [1 - exp(b \cdot \xi)] \tag{19}$$

213 *(c) Elastic behaviour*

$$\begin{bmatrix} d\varepsilon_v^e \\ d\varepsilon_q^e \end{bmatrix} = \begin{bmatrix} \frac{1}{K} & \\ & \frac{1}{3G_0} \end{bmatrix} \begin{bmatrix} dp^* \\ dq \end{bmatrix} \tag{20}$$

$$K = \frac{(1+e)p^*}{\kappa} \tag{21}$$

$$G_0 = \frac{C_0}{(1+e)^{-3}} \left(\left(\frac{p^*}{p_r} \right)^{0.5} + n_s \xi^{0.5} \right) \tag{22}$$

214 *(d) Image stress*

$$p_i^* = \frac{\left(p^* - p_{\alpha,\xi}^*\right)}{R} + \frac{p_{0,\xi}^*}{2} \tag{23}$$

$$q_i = \frac{\left(q - q_{\alpha,\xi}\right)}{R} \tag{24}$$

215 *(d) Flow rule*

$$\frac{d\varepsilon_q^p}{d\varepsilon_v^p} = \frac{\partial F_{EB}/\partial q}{\partial F_{EB}/\partial p^*} = \frac{(q - q_\alpha)/M^2}{p^* - p_\alpha^*} \tag{25}$$

216 *(e) Main drying and wetting curves*

$$S_r = \left(1 + \left(\frac{se^\psi}{\omega_d} \right)^{\frac{1}{m\psi}} \right)^{-m} \tag{26}$$

$$S_r = \left(1 + \left(\frac{se^\psi}{\omega_w} \right)^{\frac{1}{m\psi}} + C_w \right)^{-m} \tag{27}$$

Notation

a, b	parameters describing effects of ξ on NCL of soil at unsaturated state
C_0	parameter describing effects of soil structure on G_0
C_w	parameter correcting the maximum S_r of the main wetting curve
$d_1, d_{1,max}$	mapping distance and maximum mapping distance
e, e_s	void ratio and void ratio at saturated state
e_0	initial void ratio
D	vector connecting the current stress on the EB to the image stress on the BS
F_{BS}, F_{EB}	functions of the BS and the EB
G_0	elastic shear modulus
H	additional hardening modulus quantity
h, h_0	plastic hardening moduli and plastic hardening moduli when the BS and the EB are in contact
K	elastic bulk modulus
M	critical state stress ratio
m	parameter describing slope of SWRC
N_ξ, N	intercepts of NCL at a given ξ and at saturated state
n_s	parameter describing effects of ξ on G_0
p^*, q	average skeleton and deviatoric stress
(p_α^*, q_α)	centre of EB
(p_i^*, q_i)	image stress point on BS
$p_{0,\xi}^*$	yield stress at a given ξ
p_r	atmospheric pressure
R, R_ξ	the ratio between the size of EB to that of the BS

r	the radius of spherical particles which is assumed to be equal to 1x10^{-6} m
S	quantity describing the translation distance of the EB along vector D
S_r	degree of saturation
S_{rr}	degree of saturation at s_r
s	suction
s_d, s_w	image suctions on SWRC
s_r	last suction reversal
T_s	surface tension coefficient of water which is equal to 72.8 mN/m at 20°C
α	parameter describing effects of ξ on H
β	parameter describing effects of mapping distance on a change in S_r
δ	parameter describing effects of structure on H
ε_v^e, ε_q^e	elastic volumetric and deviatoric strains
λ_ξ, λ	slopes of NCL at a given ξ and at saturated state
κ	slope of URL
ϕ	parameter describing effects of mapping distance on H
ψ	Parameter describing effects of void ratio on SWRC
ω_d, ω_w	parameters describing air entry values on SWRC
ξ	bonding variable

References

Alonso, E.E., Gens, A. and Josa, A. 1990. A constitutive model for partially saturated soils. Géotechnique, **40**(3): 405-430.

Alonso, E.E., Pinyol, N.M. and Gens, A. 2013. Compacted soil behaviour: Initial state, structure and constitutive modelling. Géotechnique, **63**(6): 463-478.

Al-Sharrad, M.A. and Gallipoli, D. 2014. An elasto-plastic model for unsaturated soils with evolving anisotropy. *In* Proceedings of the 6th International Conference on Unsaturated Soils, Sydney, Australia, pp. 433–439.

Al-Tabbaa, A. and Wood, D.M. 1989. An experimentally based bubble model for clay. *In* Proceedings of the 3rd Conference on Numerical Models in Geomechanics, NUMOG III, Niagara Falls, Canada, pp. 91-99.

Chiu, A.C.F., and Ng, C.W.W. (2003). A state-dependent elasto-plastic model for saturated and unsaturated soils. *Géotechniqu*e, 53(9): 809–829.

Dafalias Y.F. 1986. Bounding surface plasticity. I: Mathematical foundation and hypoplasticity. Journal of Engineering Mechanics, **112(**9): 966-987.

D'Onza, F., Gallipoli, D. and Wheeler, S.J. 2011. Effect of anisotropy on the prediction of unsaturated soil response under triaxial and oedometric conditions: *In* Proceedings of the 5th International Conference on Unsaturated Soils, Barcelona, Spain, pp. 787–794.

Gallipoli, D. 2012. A hysteresis soil-water retention model accounting for cyclic variations of suction and void ratio. Géotechnique, **62**(7): 605-616.

Gallipoli, D., Bruno, A.W., D'Onza, F. and Mancuso, C. 2015. A bounding surface hysteretic water retention model for deformable soils. Géotechnique, **65**(10): 793-804.

Gallipoli, D., Gens, A., Sharma, R. and Vaunat, J. 2003. An elasto-plastic model for unsaturated soil incorporating the effects of suction and degree of saturation on mechanical behaviour. Géotechnique, **53**(1): 123-135.

Gallipoli, D., Wheeler, S.J. and Karstunen, M. 2003. Modelling the variation of degree of saturation in a deformable unsaturated soil. Géotechnique, **53**(1): 105-112.

Lai, B.T., Wong, H., Fabbri, A. and Denis, B. 2016. A new constitutive model of unsaturated soils using bounding surface plasticity (BSP) and non-associative flow rule. Innovative Infrastructure Solutions, **1**(3): 1-8.

Li, J., Yin, Z.Y., Cui, Y. and Hicher, P.Y. 2017. Work input analysis for soils with double porosity and application to the hydromechanical modeling of unsaturated expansive clays. Canadian Geotechnical Journal, **54**(2): 173-187.

Lloret-Cabot, M. Wheeler, S.J. and Sánchez, M. 2017. A unified mechanical and retention model for saturated and unsaturated soil behaviour. Acta Geotechnica, **12**(1): 1-21.

Niemunis, A. and Herle, I. 1997. Hypoplastic model for cohesionless soils with elastic strain range. Mechanics of Cohesive-frictional Materials, **2**(4): 279-299.

Ng, C.W.W. and Xu, J. 2012. Effects of current suction ratio and recent suction history on small-strain behaviour of an unsaturated soil. Canadian Geotechnical Journal, **49**(2): 226-243.

Ng, C.W.W., Lai, C.H. and Chiu, C.F. 2012. A modified triaxial apparatus for measuring the stress path-dependent water retention curve. Geotechnical Testing Journal, **35**(3): 490-495.

Ng, C.W.W. and Yung, S.Y. 2008. Determination of the anisotropic shear stiffness of an unsaturated decomposed soil. Géotechnique, **58**(1): 23-35.

Stallebrass, S. E., & Taylor, R. N. (1997). The development and evaluation of a constitutive model for the prediction of ground movements in overconsolidated clay. *Géotechnique*, 47(2): 235-253.

Stropeit, K., Wheeler, S.J. and Cui, Y.J. 2008. An anisotropic elasto-plastic model for unsaturated soils. *In* Proceedings of 1st European Conference on Unsaturated Soils, Durham, UK, pp. 625–631.

Wheeler, S.J., Sharma, R.S. and Buisson, M.S.R. 2003. Coupling of hydraulic hysteresis and stress-strain behaviour in unsaturated soils. Géotechnique, **53**(1): 41-54.

Wong, K.S. and Masin, D. 2014. Coupled hydro-mechanical model for partially saturated soils predicting small strain stiffness. Computer and Geotechnics, **61**(1): 355-369.

Zhou, A. and Sheng, D. 2015. An advanced hydro-mechanical constitutive model for unsaturated soils with different initial densities. Computer and Geotechnics, **63**(1): 46-66.

Zhou, A., Sheng, D. Sloan, S.W. and Gens, A. 2012. Interpretation of unsaturated soil behaviour in the stress-saturation space, I: volume change and water retention behaviours. Computer and Geotechnics, **43**(1): 178-187.

Zhou, C., Ng, C.W.W. and Chen, R. 2015a. A bounding surface plasticity model for unsaturated soil at small strains. International Journal for Numerical and Analytical Methods in Geomechanics, **39**(11): 1141-1164.

Zhou, C., Xu, J. and Ng, C.W.W. 2015b. Effects of temperature and suction on secant shear modulus of unsaturated soil. Géotechnique Letter, **5**(3): 123-128.

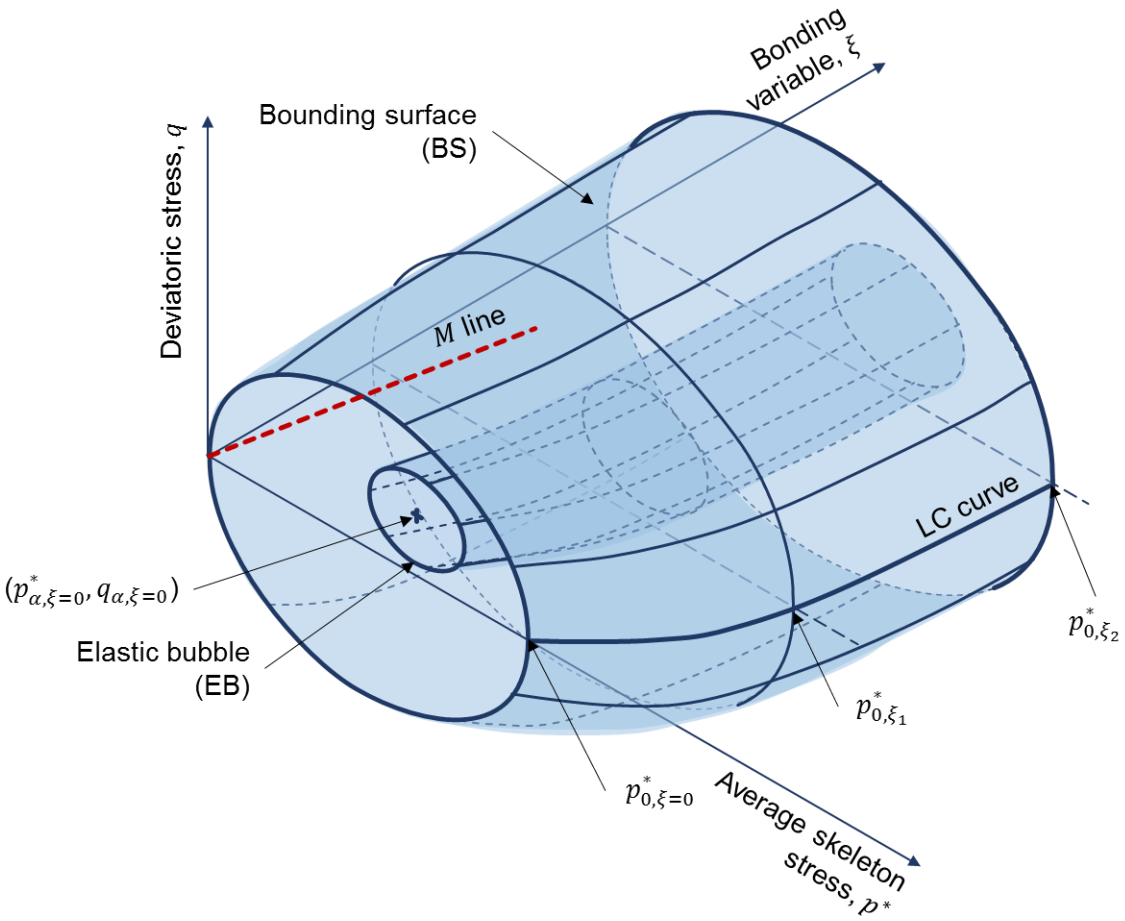

Figure 1. Schematic diagram of the elastic bubble and bounding surface in the $p^* - q - \xi$ space

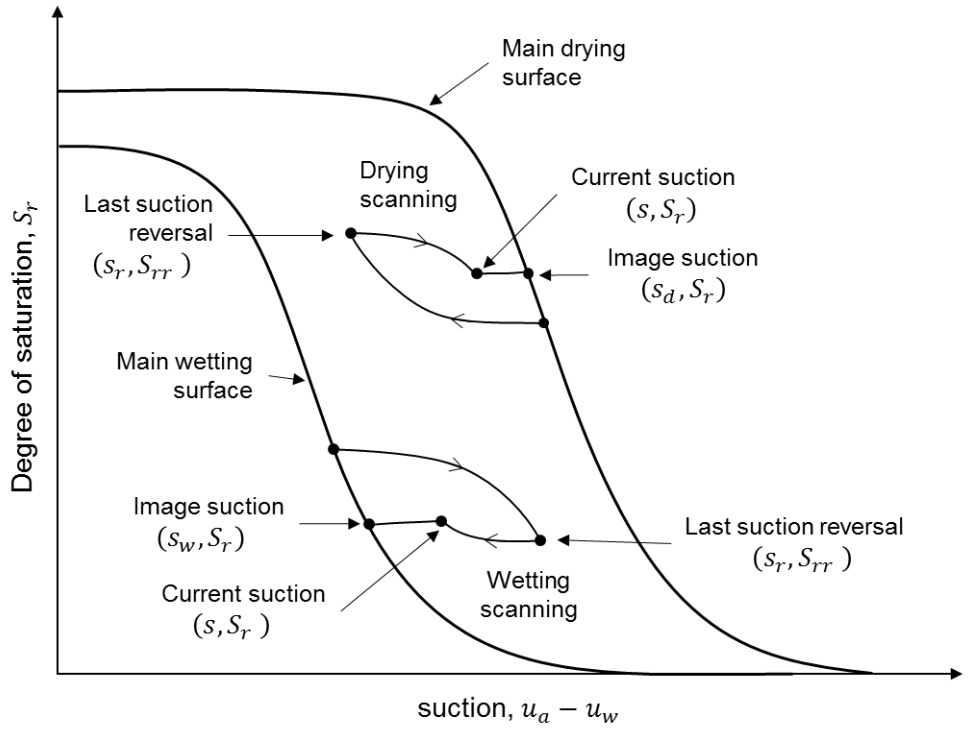

Figure 2. Modelling water retention behaviour using bounding surface plasticity framework

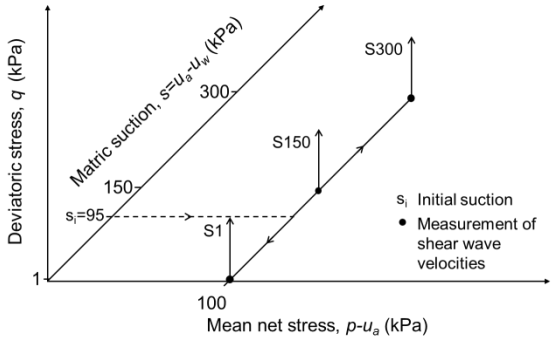

(a)

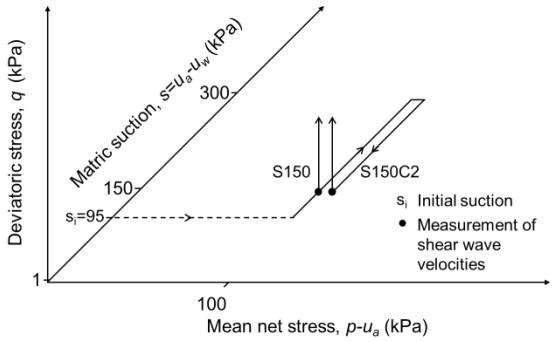

(b)

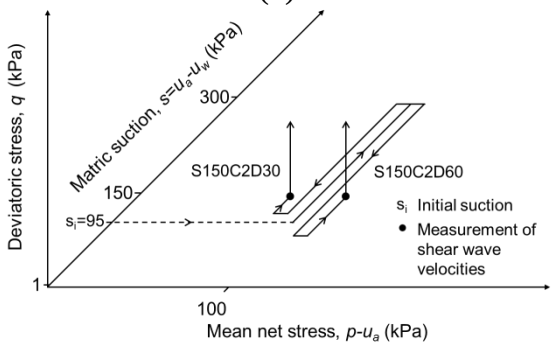

(c)

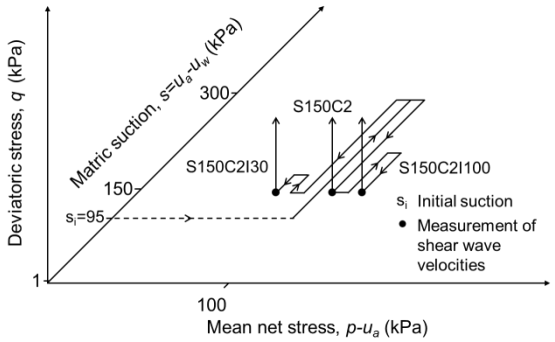

(d)

Figure 3. Stress paths of test series for investigating (a) effect of suction (b) effect of suction history (c) effect of recent wetting-drying history and (d) effect of recent drying-wetting history on small strain stiffness of CDT

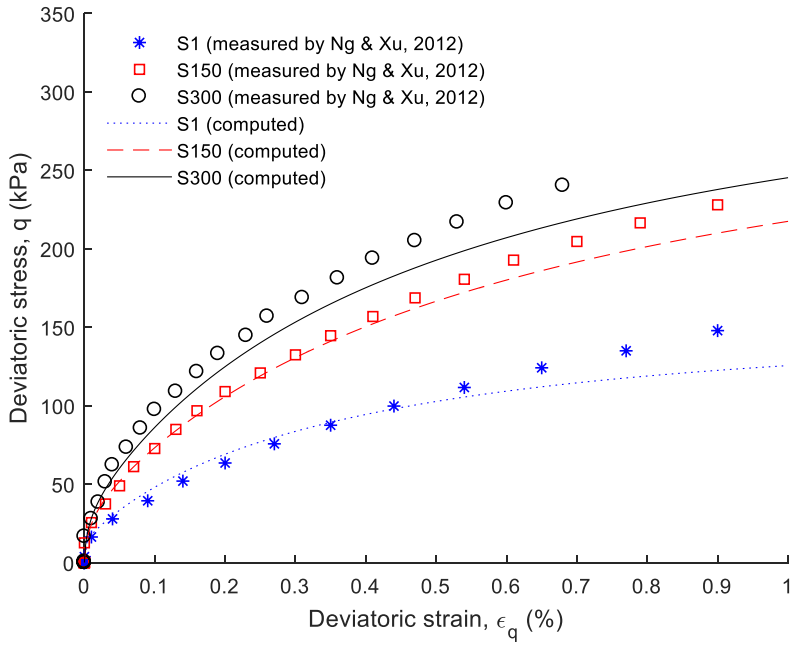

(a)

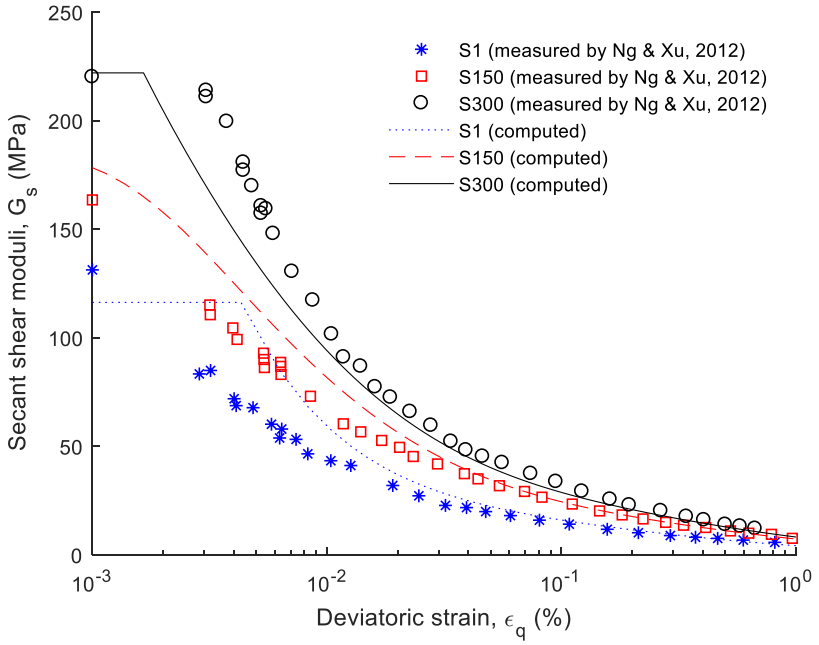

(b)

Figure 4. Comparisons between measured and computed suction effects on (a) stress-strain relations and (b) stiffness degradation of CDT

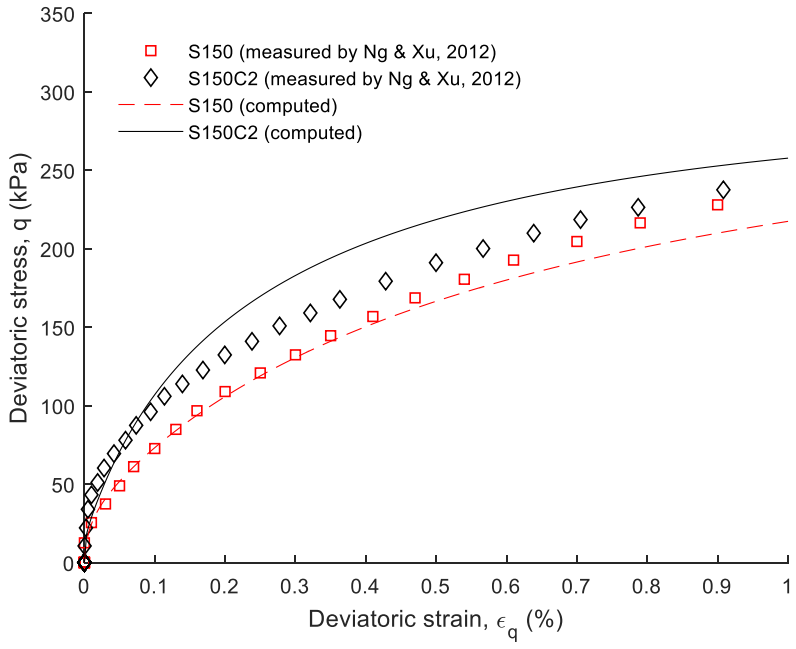

(a)

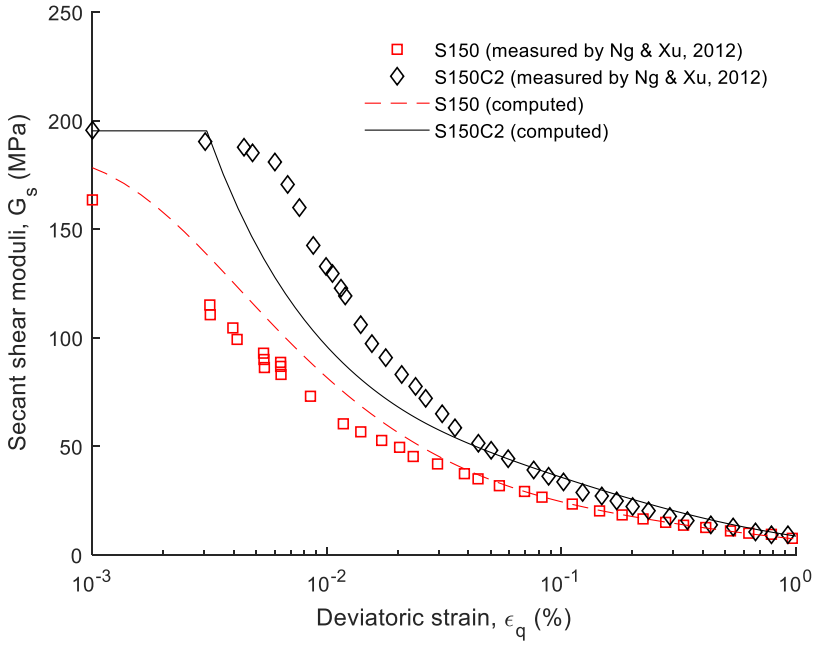

(b)

Figure 5. Simulating the influence of suction history on (a) stress-strain relations and (b) stiffness degradation of CDT

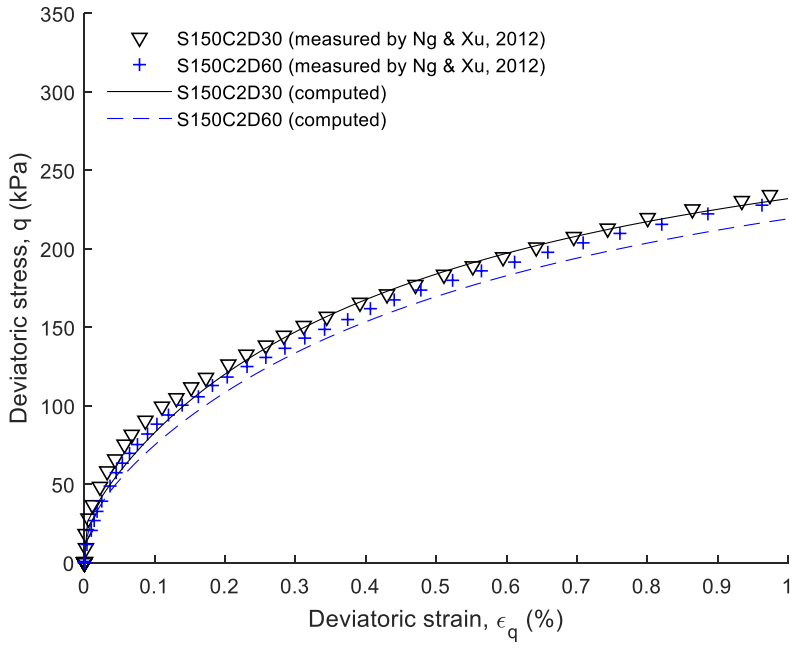

(a)

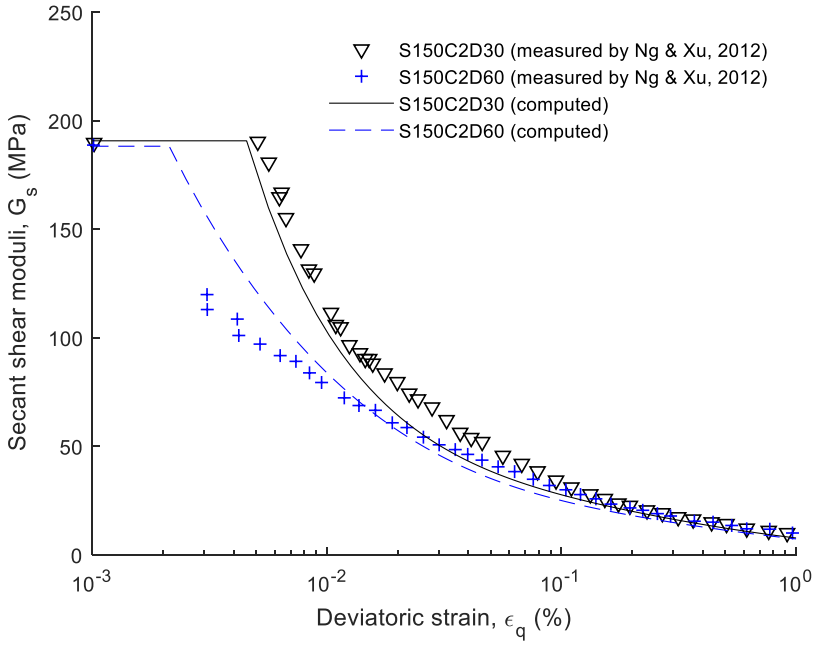

(b)

Figure 6. Effects of recent wetting-drying history on (a) stress-strain relations and (b) stiffness degradation of CDT

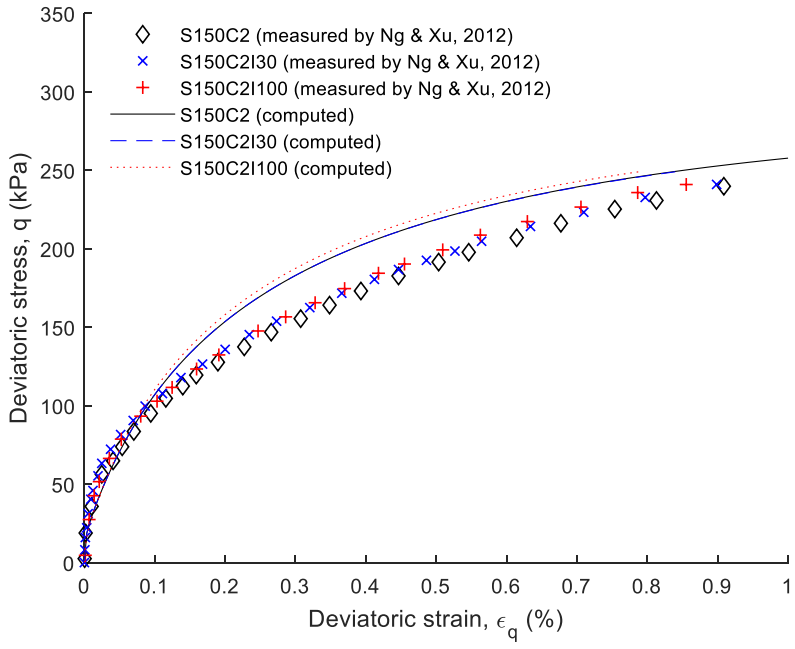

(a)

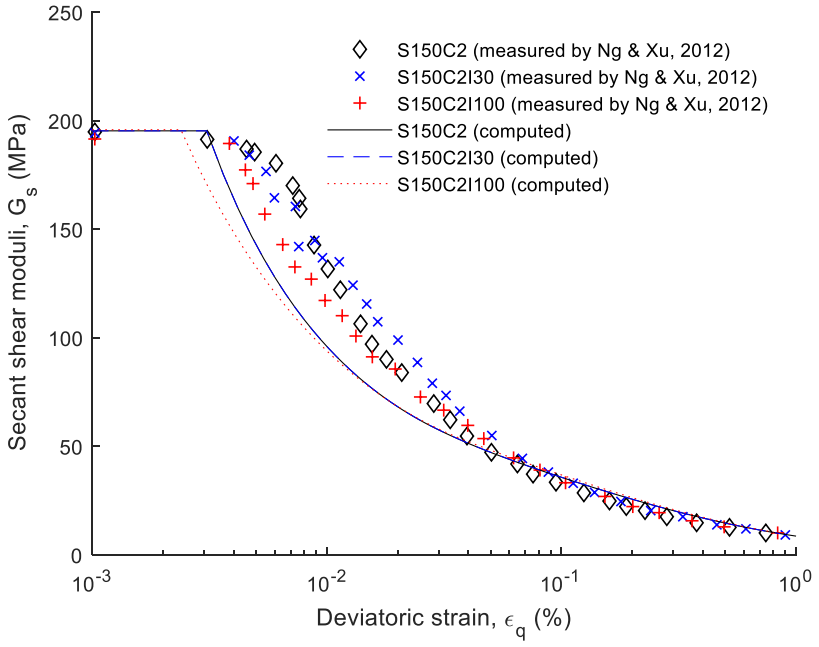

(b)

Figure 7. Effects of recent drying-wetting history on (a) stress-strain relations and (b) stiffness degradation of CDT

Table 1. Basic properties of CDT (data from Ng & Xu, 2012)

Property	Value
Soil type (ASTM, 2006)	Silt (ML)
Specific gravity, G_s	2.73
Particle-size distribution (%)	
Clay fraction	24
Silt fraction	72
Sand fraction	4
Atterberg limits (%)	
Liquid limit	43
Plasticity index	14
Maximum dry density (g/cm^3)	1.76
Optimum water content (%)	16.3

Table 2. Summary of model parameters for CDT

Soil parameter		Value
Isotropic compression		
κ	slope of URL	0.010
N	intercept of NCL at a reference pressure (100 kPa)	1.65
λ	slope of NCL	0.085
Critical state		
M	critical state stress ratio	1.42
Suction hardening		
a	parameter describing effects of ξ on e/e_s	-0.2
b	parameter describing effects of ξ on e/e_s	-7
Hydraulic properties (SWRC)		
m	parameter describing slope of SWRC	0.99
n	parameter describing slope of SWRC	1.88
ω_d	parameter describing AEV of main drying curve	178
ω_w	parameter describing AEV of main wetting curve	50
C_w	parameter describing maximum S_r of main wetting curve	0.1
β	parameter describing scanning curve	1.7
Elastic shear modulus		
C_0	parameter describing effects of structure on G_0	330
n_s	parameter describing effects of ξ on G_0	1.2
Elastic domain		
R	ratio of the size of EB to that of BS	0.08
Hardening modulus (H)		
δ	parameter describing effects of structure on H	0.03
ϕ	parameter describing degradation of H	1.5
α	parameter describing effects of ξ on H	0.22